A timescale investigation of volatile chemical retention during hydrometeor freezing: Nonrime freezing and dry growth riming without spreading

A. L. Stuart[1] and M. Z. Jacobson

Department of Civil and Environmental Engineering, Stanford University, Stanford, California, USA

Received 18 October 2001; revised 12 April 2002; accepted 22 November 2002; published 19 March 2003.

[1] Partitioning of volatile chemicals among the gas, liquid, and solid phases during the conversion of liquid water to ice in clouds can impact the poststorm distributions of chemicals in the troposphere and in precipitation. In this paper, we use a timescale-based methodology to determine the key physical parameters involved in retention and derive the dependence of retention on these parameters for nonrime freezing and rime freezing when droplet spreading is minimal. We calculate a dimensionless retention indicator for SO_2, H_2O_2, NH_3, and HNO_3, for a variety of conditions relevant to natural clouds. We find that solute properties, particularly the effective Henry's constant, likely have a large impact on retention. Chemicals with very high effective Henry's constants (e.g., HNO_3) will likely be retained completely under all conditions. For chemicals with lower effective Henry's constants, freezing conditions (including pH, temperature, magnitude of the hydrometeor velocity in air, and drop size) will likely have significant impacts on retention, while air pressure has only a small effect. The dependence on velocity and drop size depends on the limiting mass transport regime and is nonmonotonic due to the competing effects of ventilation on heat and mass transport. The formation of a complete or partial ice shell likely also affects retention significantly. Comparison of our results with available experimental data provides possible explanations of the trends and apparent disagreement found in the studies. The theory-based analysis and methodology presented in this paper can be used to improve experimental design and parameterization of retention in cloud models. *INDEX TERMS:* 0320 Atmospheric Composition and Structure: Cloud physics and chemistry; 0365 Atmospheric Composition and Structure: Troposphere—composition and chemistry; 0368 Atmospheric Composition and Structure: Troposphere—constituent transport and chemistry; 3354 Meteorology and Atmospheric Dynamics: Precipitation (1854); *KEYWORDS:* ice chemistry, precipitation chemistry, cloud chemistry, gas scavenging, chemical partitioning, freezing

Citation: Stuart, A. L., and M. Z. Jacobson, A timescale investigation of volatile chemical retention during hydrometeor freezing: Nonrime freezing and dry growth riming without spreading, *J. Geophys. Res.*, *108*(D6), 4178, doi:10.1029/2001JD001408, 2003.

1. Introduction

[2] Convective clouds significantly impact tropospheric chemistry and chemical deposition to the ground by moving trace gas species from the boundary layer to the free troposphere and through chemical scavenging by cloud hydrometeors. Interactions between trace chemicals and the ice phase are not well understood despite the presence of ice in many cloud systems. Chemical interactions with ice in clouds include surface adsorption, codeposition, multicomponent nucleation, surface reactions, and chemical phase partitioning during shock freezing of liquid hydrometeors. In this paper, we focus on developing an understanding of the latter phenomena.

[3] Collision of supercooled water with ice and subsequent freezing to form graupel and hail is an important mechanism of precipitation development in cold clouds. Chemical solutes originally dissolved in a supercooled water drop may be retained or expelled from the hydrometeor as it freezes. The degree of retention will affect a chemical's availability for gas- and aqueous-phase reactions and its movement in the cloud. Cloud modeling studies that have examined the effects of this phenomena have found that it may significantly impact a chemical's distribution in the troposphere and deposition to the ground [*Barth et al.*, 2001; *Audiffren et al.*, 1999; *Wang and Chang*, 1993; *Chen and Lamb*, 1990; *Cho et al.*, 1989]. We need to understand and predict freezing retention in order to quantify its effects on acid deposition and the chemistry of the troposphere.

[4] During freezing of aqueous solutions, solutes are retained to differing degrees depending on the characteristics of the solute and the conditions of freezing. Freezing

[1]Now at Center for International Security and Cooperation, Stanford University, Stanford, California, USA.

0148-0227/03/2001JD001408$09.00

leads to efficient retention of nonvolatile species such as sulfate [e.g., *Borys et al.*, 1982; *Mitchell and Lamb*, 1989]. The degree of retention of more volatile species is not well characterized. Several laboratory and field studies have measured retention efficiencies of gases found in clouds, including H_2O_2, SO_2, O_2, HCl, NH_3, and HNO_3 [e.g., *Lamb and Blumenstein*, 1987; *Iribarne and Pyshnov*, 1990; *Snider et al.*, 1992; *Voisin et al.*, 2000]. The retention efficiency is the ratio of solute mass in the hydrometeor after freezing to the mass originally dissolved in the droplet. Measured retention efficiencies range from 0.01 to 1. The reasons for the differing values are not well understood. Several factors varied among studies, including temperature, droplet and substrate size, solute concentration, pH, and drop ventilation conditions. Two studies found retention efficiency to be inversely related to freezing temperature [*Lamb and Blumenstein*, 1987; *Iribarne et al.*, 1990]. There is limited theoretical explanation available for the differences, with contradictory theories proposed by different authors. Since the experimental data are limited, apparently inconsistent, and poorly understood, they cannot be used with confidence in cloud modeling simulations.

[5] To understand freezing retention and apply experimental data in cloud models, a theoretical understanding of the interactions between the physical and chemical processes involved in freezing retention of volatile species is needed. In this work, we develop a theory-based timescales method for examining retention and its dependence on freezing conditions and solute properties. We apply this method to investigate retention of volatile solutes during nonrime freezing of supercooled drops in clouds and rime freezing under conditions where spreading of drop water on impact with the rimer is minimal.

2. Development of a Theory-Based Indicator of Retention

[6] When freezing nucleation occurs in a supercooled solution, it initiates crystal growth. A growing crystal interface incorporates solute molecules to a degree dependent on the thermodynamics of phase transformation, which are highly dependent on solution composition [*Wolten and Wilcox*, 1967]. The physical chemistry of freezing nucleation in concentrated aqueous solutions is an active area of current research [*Clapp et al.*, 1997; *Tabazadeh and Toon*, 1998; *Bertram et al.*, 2000]. In dilute solutions, such as cloud and rain drops with radii greater than 1 μm, ice is known to be very exclusionary of most solutes (i.e., solute solubility in ice is very small) (see *Hobbs* [1974, pp. 600–602] for a review). For nonvolatile species, solute exclusion from ice causes concentrations in the liquid to increase. This leads to increasing solute concentrations in ice as the ice interface grows. After freezing, the solute distribution in ice is inhomogeneous, but the overall solute concentration in ice is the same as in the original hydrometeor [e.g., *Pfann*, 1966]. For volatile species, solute may leave the solution either through the air/liquid interface, or through bubble formation at the solid/liquid interface [*Wilcox*, 1967]. The exclusion of solute from ice sets up a concentration gradient in the remaining solution, which drives solute transfer away from the solid/liquid interface and into the gas phase. This provides a mechanism for lower solute concentration in the final ice solution than the original liquid solution. However, since ice-liquid partitioning depends on the concentration at the ice/liquid interface, if solute movement away from the interface proceeds slowly compared to the rate of interface advance, solute concentration in the solid phase increases (similar to the nonvolatile solute). In addition, supercooling of the liquid phase leads to dendritic crystal growth [e.g., *Hobbs*, 1974, pp. 572–575]. Dendritic growth causes the build-up of solute in dendrite valleys and entrapment of higher concentrations of solute in the frozen ice than is thermodynamically favorable [e.g., *Harrison and Tiller*, 1963; *Edie and Kirwan*, 1973]. Finally, chemical diffusion coefficients in solid ice are orders of magnitude smaller than those in water [e.g., *Sommerfeld et al.*, 1998; *Thibert and Dominé*, 1998], so the nonequilibrium gas-ice chemical distribution can be maintained after freezing. Therefore, partitioning during shock freezing of cloud hydrometeors is likely more a function of kinetics than of ice-liquid or ice-gas thermodynamics.

[7] Redistribution of solutes by freezing of water systems has been studied by many authors [e.g., *Gross et al.*, 1977; *Baker*, 1967; *Tiller and Sekerka*, 1964; *Myerson and Kirwan*, 1977], but no universal theory applicable to dendritic freezing, has yet been developed. We focus on developing a scaling approach. Figure 1 provides an idealized depiction of the two categories of processes (crystal growth and solute expulsion) involved in volatile solute retention relevant for freezing of a supercooled drop. Crystal growth and solute expulsion are the result of the coupling of several heat and mass transfer processes. As a tool to simplify and analyze the coupling of processes involved in retention during freezing, we use a resistance (circuit) analogy, representing crystal growth and solute expulsion as parallel phenomena.

[8] Comparing timescales of the underlying processes involved, we can improve our understanding of the conditions that affect retention and can develop an indicator of retention. For volatile solutes, we expect that the amount of retention will depend on the rate of solute transfer versus the rate of freezing. Using our resistance model we develop overall timescales (or inverse rates) for both freezing and solute expulsion. By taking the ratio of the expulsion timescale (τ_{exp}) to the freezing timescale (τ_{frz}), we define the dimensionless group τ_{exp}/τ_{frz}, and call it the retention indicator. For $\tau_{exp}/\tau_{frz} \gg 1$, we expect retention to be complete. For $\tau_{exp}/\tau_{frz} \ll 1$, we expect loss to be complete. For τ_{exp}/τ_{frz} on the order of 1, we expect this group to be to be directly related to retention.

3. Timescales of Involved Processes

[9] To determine the retention indicator, we need timescales representative of crystal growth (freezing) and solute expulsion. For the drop freezing timescale, we use estimated freezing times based on equations available in the literature. For the solute expulsion timescale we use the characteristic times for the underlying mass transfer processes. Physically, the characteristic time is effectively the time it would take to reduce the solute concentration in the drop by $1/e$ its original value in an open system.

3.1. Freezing Timescale

[10] Ice-phase hydrometeors can form and grow due to freezing of supercooled water under a variety of conditions

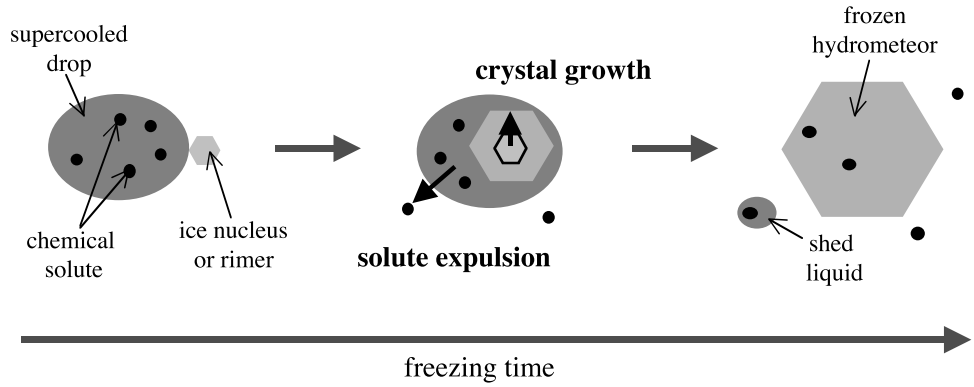

Figure 1. Idealized depiction of the phenomena involved in retention during freezing. The left cartoon depicts the distribution of solute just prior to a freezing nucleation event. The center cartoon depicts the ice crystal growth and solute expulsion phenomena occurring during freezing. The right cartoon depicts the distribution of solute once the drop has frozen.

and geometries. Freezing in clouds can be divided into two general categories depending on the mechanism inducing freezing: (1) nonrime freezing, which is initiated by homogeneous or heterogeneous nucleation, and (2) riming, which is initiated by aggregation of supercooled water drops and ice hydrometeors. The analysis in this paper assumes minimal drop spreading (drops freeze in the approximate shape as the original hydrometeor), individual drop freezing (no coalescence or interference by other drops), and heat loss predominantly to air. These criteria hold for nonrime freezing and for dry growth riming at low temperatures, low impact velocities, and small drop sizes [*Pruppacher and Klett*, 1997, p. 660; *Macklin and Payne*, 1967, 1969]. Specifically, *Griggs and Choularton* [1983] found that during dry growth riming at temperatures less than -10°C and impact speeds of about 2 m/s, drops freeze symmetrically inward (indicating predominant heat loss to air) in approximately spherical shape with little contact with the substrate. *Macklin and Payne* [1968] found coalescence and interference from other drops unlikely, except at substrate temperatures within a few degrees of 0°C.

[11] For both categories of freezing, solidification of supercooled water drops occurs in approximately two stages, the adiabatic and diabatic stages [*Pruppacher and Klett*, 1997, pp. 674–675]. During the adiabatic stage, only a very small fraction of the drop solidifies as ice dendrites radiate out from the nucleation site [*Hobbs*, 1974, p. 572]. Most of the released latent heat of freezing contributes to warming the liquid water in the drop to approximately 0°C, and little heat is released into the drop environment. (Hence, the loose application of the term "adiabatic.") Subsequent freezing in the diabatic stage is controlled by the rate of latent heat dissipation by both conduction into the frozen ice substrate and by heat transfer to the drop environment (air). For conditions applicable to this study, ice shell formation soon after the adiabatic stage may significantly limit solute transfer. However, the ice shell may be incomplete or fissures may form [*Griggs and Choularton*, 1983], providing a mechanism for solute removal throughout the diabatic stage. The diabatic freezing time is generally one or more orders of magnitude longer than the adiabatic freezing time and hence, the total freezing time is generally considered approximately equal to the diabatic freezing time [*Pruppacher and Klett*, 1997, p. 675]. The freezing time for each of these stages can be considered the bounding values for the freezing time relevant to solute retention. If a complete ice shell forms immediately after the adiabatic stage, the adiabatic freezing time will limit solute transfer. If no ice shell forms, the diabatic freezing time will limit solute transfer. If an ice shell forms sometime during diabatic freezing, the freezing time (and hence the retention indicator) will be an intermediate value between these two extremes. Therefore, in our analysis of retention indicator, we consider both the adiabatic and diabatic freezing timescales as limits to volatile solute loss.

3.1.1. Adiabatic Freezing

[12] Following the development of *Macklin and Payne* [1967], the adiabatic freezing time can be approximated by the time it takes for ice dendrites to penetrate through the supercooled drop. This timescale is estimated as $\tau_{f-ad} = \frac{a}{G}$, where G is the intrinsic growth rate of ice in supercooled water. Experimental and theoretical studies indicate an approximate dependence on ΔT_∞ [*Pruppacher and Klett*, 1997, pp. 673, 668]. Substituting this dependence into τ_{f-ad} gives

$$\tau_{f-ad} \approx \frac{a}{c'(\Delta T_\infty)^2} \text{ for } 0 \gtrsim T_\infty > -10^{\circ}\text{C} \tag{1a}$$

$$\tau_{f-ad} \approx \frac{a}{c''\Delta T_\infty} \text{ for } T_\infty \lesssim -10^{\circ}\text{C} \tag{1b}$$

where c' and c'' are constants. Based on observed data on growth rates [*Pruppacher and Klett*, 1997, p. 669], here we used values of 0.05 and 0.6, respectively.

3.1.2. Diabatic Freezing

[13] By balancing heat generated by freezing with that dissipated to air, *Pruppacher and Klett* [1997, pp. 677–679] developed an equation for the diabatic freezing time of droplets falling freely in air:

$$\tau_{f-d} = \frac{\rho_w L_m a^2 [1 - \Delta T_\infty c_w / L_m]}{3\bar{F}_g \Delta T_\infty \left[k_a + L_s D_v \overline{\left(\frac{d\rho_v}{dT}\right)}_{\text{sat,i}}\right]} \tag{2}$$

where a is the drop radius, ΔT_∞ is the difference between the supercooled drop temperature and the equilibrium

freezing temperature of water ($0°C - T_\infty$), ρ_w is the density of the supercooled water, L_m is the latent heat of ice melting, c_w is the specific heat of water, $\bar{F}_g$ is the mean ventilation coefficient for heat and mass transfer in the gas phase, k_a is the thermal conductivity of air, L_s is the latent heat of sublimation of water vapor, D_v is the diffusivity of water vapor in air, and $\overline{(d\rho_v/dT)}_{sat,i}$ is the mean slope of the ice saturation vapor density curve over the temperature interval from the surface temperature of the freezing drop to T_∞.

[14] Equation (2) neglects heat dissipation to the underlying solid substrate and assumes that the drop freezes in a spherical shape. For nonrime freezing these conditions are approximately correct, since the size of the underlying substrate (if it exists) is very small and drops are known to freeze in the approximate shape of the original drop [*Hobbs*, 1974]. For rime freezing, the underlying substrate can contribute to heat dissipation depending on its size, temperature, and thermal properties [*Macklin and Payne*, 1967, 1968; *Baker et al.*, 1987]. The shape of the drop undergoing rime freezing will depend on the degree of spreading, which ultimately depends upon freezing temperatures (substrate and drop) and impact speed [*Macklin and Payne*, 1967, 1969]. For drops for which spreading and heat loss are significant, the diabatic freezing time will be reduced. Equation (2) has been found to provide estimates which agree well with available experimental data for drops suspended in air [*Pruppacher and Klett*, 1997, p. 679].

3.2. Volatile Solute Expulsion Timescale

[15] During crystal growth, solutes may be removed from the hydrometeor through solute transport in the condensed-phase, across the liquid-air interface, and in the gas-phase. Here we consider only processes of translational mass transfer. Reaction processes will affect the overall fate of any element by changing the physical and chemical properties (e.g., diffusivities, volatility, ice/liquid interfacial distribution coefficient, etc.) of the parent species. The impact of these processes is discussed in section 8.

[16] The characteristic time for gas-phase mass transfer to or from a spherical particle [*Schwartz*, 1986; *Pruppacher and Klett*, 1997, p. 775] is given by

$$\tau_g = \frac{a^2 H^*}{3 D_g F_m}, \tag{3}$$

where D_g is the diffusivity of the chemical in air. H^* is the effective concentration Henry's law constant (unitless) that accounts for dissociation; $H^* = \beta K_H RT$, where K_H is the Henry's constant (M/atm), β is the dissociation factor, and R is the universal gas constant. F_m is the gas-phase ventilation coefficient for mass transfer of the chemical, enhanced due to air flow around the droplet.

[17] The characteristic time for liquid/gas interfacial mass transport for a spherical drop is [*Schwartz*, 1986; *Seinfeld and Pandis*, 1998, p. 613]:

$$\tau_i = \frac{4 a H^*}{3 \bar{v} \alpha}, \tag{4}$$

where $\bar{v}$ is the thermal velocity of the chemical in air and α is its interfacial mass accommodation coefficient. Accommodation coefficients have been measured for many solutes and are temperature dependent [e.g., *Davidovits et al.*, 1995]. Measured accommodation coefficients vary from about 1×10^{-4} to 0.2 [e.g., *Pruppacher and Klett*, 1997, p. 779].

[18] The characteristic time for aqueous-phase mass transport through a spherical drop is [*Schwartz*, 1986; *Seinfeld and Pandis*, 1998]

$$\tau_{aq} = \frac{a^2}{\pi^2 D_{aq} F_{aq}}, \tag{5}$$

where D_{aq} is the aqueous diffusivity of the chemical. We have added F_{aq} to the diffusive timescale to account for enhanced mass transfer in the liquid phase. The development of this ventilation coefficient is given by *Stuart* [2002]. As discussed in section 3.1, ice shell formation during freezing may limit condensed-phase solute transfer. If the shell is not complete or contains water-filled fissures, solute is transferred through this shell at a rate greater than that in solid ice. The expression for τ_{aq} can be used for condensed-phase solute transfer, but an effective diffusivity in the ice-water system replaces D_{aq}.

[19] Since these translational solute transfer processes occur in series, the overall timescale can be estimated by summing the timescales of individual processes or by determining the limiting (longest) timescale.

4. Functional Dependence of Retention on Process Variables

[20] To determine the likely functional dependence of retention on conditions, we derived analytical expressions for the retention indicator, τ_{exp}/τ_{frz}. Expressions were derived for several different categories of conditions by taking the ratio of the limiting solute expulsion time for each type of solute transfer control to the adiabatic and diabatic freezing time, respectively. Table 1 provides a summary of the conditions for which each solute transfer and freezing process may be most important (possibly controlling) to solute retention during freezing. Tables 2, 3, and 4 give a summary of the dependence of the retention indicator on the key variables: solute properties, temperature, and ventilation conditions, respectively. The derivation of the expressions listed in these tables is given by *Stuart* [2002].

5. Quantifying the Retention Indicator

[21] To quantify our retention indicator and explore its dependence on ambient conditions and solute porperties, we calculated τ_{exp}/τ_{frz} for numerous cases. These included a typical nonrime freezing case and a dry growth riming case for which spreading would be expected to be minimal. We also calculated the retention indicator for cases with each of the independent parameters varied independently within the range appropriate for hydrometeor freezing in clouds.

[22] For all cases, we considered ten discrete drop sizes representing small cloud drops through large rain drops (1, 5, 10, 25, 50, 100, 250, 500, 1000, and 2000 μm). Properties of water phase change, supercooled water, moist air, and ice were calculated as functions of the temperature using avail-

Table 1. Conditions for Which Each Solute Transfer and Freezing Process May be Most Important (Possibly Controlling) to Solute Retention During Freezing

Process	Expression	Description
		Freezing
Adiabatic		lower temperatures, lower impact speeds, smaller drops, smaller ice substrates, higher ventilation
Diabatic		higher temperatures, higher impact speeds, larger drops, larger ice substrates, lower ventilation
		Solute Transfer
Gas-phase	$\frac{D_{aq}F_{aq}H^*}{D_gF_m} \gg 1,\ \frac{a\bar{v}\alpha}{D_gF_m} \gg 1$	relatively soluble chemicals ($K_H^* \gtrsim 1 \times 10^4$ M/atm) for F_{aq}, $F_m \approx 1$, intermediate pHs for chemicals studied, (lower velocities, larger drops)
Interfacial	$\frac{D_{aq}F_{aq}H^*}{a\bar{v}\alpha} \gg 1,\ \frac{D_gF_m}{a\bar{v}\alpha} \gg 1$	most important for very small α ($\alpha \lesssim 1 \times 10^{-3}$) or very small drops ($a \lesssim 10$ μm)
Condensed-phase	$\frac{D_gF_m}{D_{aq}F_{aq}H^*} \gg 1,\ \frac{a\bar{v}\alpha}{D_{aq}F_{aq}H^*} \gg 1$	very volatile chemicals, pH dependent(SO_2: pH $\lesssim$ 3; NH_3: pH $\gtrsim$ 10), very small D_{aq} (e.g. if ice impedes transfer), (intermediate to high velocities, small to intermediate drop sizes)

able literature correlations. The density of the ice formed was assumed to be that of pure ice at 0°C. A sensitivity study indicated that this assumption had no impact on the results.

[23] To calculate solute mass transfer timescales, properties of the volatile solute are needed. We considered four chemicals of interest in the cloud chemistry literature, sulfur dioxide, hydrogen peroxide, ammonia, and nitric acid. Values of Henry's constants, dissociation equilibrium constants, diffusivities, and gas-water accommodation coefficients were calculated from temperature dependent correlations available in the literature. Values at a temperature of 0°C were used since the freezing drop is at this temperature during most of the freezing process. Table 5 provides a summary of the solute property values used.

[24] Using equations (3), (4), and (5), we calculated the characteristic times for gas-phase, liquid-gas interfacial, and aqueous-phase solute mass transport, respectively, for each drop size considered. To determine the overall mass transfer timescale, τ_{exp}, we summed the individual mass transport timescales.

[25] To estimate the time for adiabatic and diabatic freezing, we used equations (1a) and (1b) and equation (2), respectively. We determined the total freezing time as the sum of the adiabatic and diabatic freezing times. Diabatic freezing times were more than an order of magnitude larger than adiabatic freezing times for all drop sizes except a = 1 μm. Hence, the total freezing time is approximately equal to the diabatic freezing time for $a \gtrsim 1$ μm.

5.1. Typical Nonrime Freezing of Drops

[26] To calculate retention indicators for typical nonrime freezing of cloud hydrometors, we assumed cloud drops freeze due to homogeneous nucleation and rain drops freeze due to heterogeneous nucleation. For ambient freezing temperatures, we used the fitting expression, $T(°C) = -39 + 3 \ln a(\mu m)$, based on available size-specific mean nucleation temperature data [*Hobbs*, 1974; *Pruppacher and Klett*, 1997]. The air temperature, supercooled drop temperature, and ice temperature were assumed equal. We used a pH of 4.0 since this is typical of the available experimental data on retention. We assumed a pressure of 300 mbar.

[27] We assumed the drops fall at their terminal velocities. Terminal fall velocities and Reynolds numbers for different size drops were determined using calculations appropriate to the flow regime (slip flow, hard sphere continuum flow, and deformed drops). To calculate the convective or turbulent enhancement to heat and mass transfer, we determined heat and mass transfer ventilation coefficients based on literature correlations, as described by *Stuart* [2002].

[28] Table 6 lists the conditions assumed and the freezing times for our nonrime freezing case. Table 7 lists the calculated mass transfer timescales and retention indicators.

Table 2. Functional Dependence of Retention Indicator on Solute Properties for Each Pair of Controlling Solute Transfer and Freezing Processes[a]

Relevant Ventilation Conditions			Adiabatic or Diabatic Freezing Control
Regime	Expression	Description	
		Gas-Phase Solute Transfer Control	
$F_m, \bar{F}_g \approx 1$	$Sc_{wv\&sol}^{1/3}Re^{1/2} \lesssim 1$	low velocities, small drops	$\sim H^*D_g^{-1}$
$F_m, \bar{F}_g \gg 1$	$Sc_{wv\&sol}^{1/3}Re^{1/2} \gtrsim 25$	high velocities, large drops	$\sim H^*D_g^{-2/3}$
		Interfacial Solute Transfer Control	
all F_m, F_{aq}	–	all ventilation conditions	$\sim H^*\alpha^{-1}$
		Aqueous-Phase Solute Transfer Control	
$F_{aq}, \bar{F}_g \approx 1$	$[Sc_{wv}$ and $Pr]^{1/3}Re^{1/2} \lesssim 1$	low velocities, small drops	D_{aq}^{-1}
$F_{aq} > 1$ (any $\bar{F}_g$)	$(Re')^2Sc' \gtrsim 900$	higher velocities, larger drops	–

[a]Conditions specified indicate general conditions for which the expression applies, if the given solute transfer process is controlling. Conditions under which each solute transfer process will be most important are given in Table 1. $Re' = Re(\eta_a/\eta_w)$, $Sc' = Sc(D_g/D_{aq})$.

Table 3. Functional Dependence of Retention Indicator on Supercooled Drop Temperature[a]

Adiabatic Freezing Control	Diabatic Freezing Control
$\sim(\Delta T_\infty)^m$	$\sim \frac{\Delta T_\infty}{[1-\Delta T_\infty c_w/L_m]}$ ($\sim\Delta T_\infty$ for $T_\infty \gtrsim -20$°C)

[a]Here, $m = 2$ or 1 for $0 \geq T_\infty \geq -10$°C and $T_\infty < -10$°C, respectively.

5.2. Dry Growth Riming Without Spreading

[29] To calculate retention indicators for our dry growth riming case, we assumed an air (and supercooled drop) temperature of −10°C, drop speed of 200 cm/s, and pressure of 700 mbar. Table 6 list the conditions assumed and the calculated freezing times for our dry growth riming case.

5.3. Variability Study

[30] To investigate the impact of solute properties and freezing conditions on retention indicator, we performed calculations with each variable varied independently. Variables we considered included those suggested by our analytical development in section 4, including drop size, hydrometeor speed in air, temperature, pressure, pH (due to its impact on effective Henry's constants), gas-water accommodation coefficient, and diffusivities. For each variable considered, we varied the value within the range of reasonable or observed conditions. Table 8 lists selected values considered for each variable considered and the general impacts of each variable on the retention indicator.

6. Results and Discussion

[31] Figures 2a and 2b show the retention indicator results for the typical nonrime freezing and dry growth riming cases, respectively. For both these cases, we see that the magnitude of the retention indicator is highly chemical specific. Due to the importance of the gas and interfacial mass transport limitations, the retention indicators scale directly with the effective Henry's constant, as specified in Table 2. H^* varied widely between the four chemicals studied (from 1.8×10^4 for SO_2 to 1.0×10^{13} for HNO_3).

[32] Although the magnitude of the retention indicators is very chemical specific, the dependence on radius is not very chemical specific for these cases. For the dry growth riming case and all chemicals studied, the gas-phase is a significant resistance to mass transfer for drops larger than about 10 μm. (The gas phase limits mass transfer for drops larger than about 25 μm for all chemicals expect SO_2.) Therefore, we see that the diabatic retention indicator is not a function of radius for $a \gtrsim 25$ μm, while the adiabatic

Table 5. Solute Properties Used for Case Calculations[a]

Property	SO_2	H_2O_2	NH_3	HNO_3
Molecular weight, g/mol	64	34	17	63
Accomodation coeff.	0.11	0.23	0.097	0.15
Gas-phase diffusivity, cm^2/s	0.16–0.35	0.24–0.53	0.3–0.68	0.15–0.34
Aqueous-phase diffusivity, cm^2/s	7.7e-6	1.1e-5	1.1e-5	7.5e-6
Henry's constant, M/atm	3.2	6.9e5	220	2.1e5
1st dissociation constant, M	0.025	5.1e-13	4.5e-6	220
2nd dissociation constant, M	1.0e-7	–	1.3e-15	–

[a]The gas-phase diffusivity used is calculated for T_{air}, hence a range of values is listed. All other temperature-dependent properties are calculated for T_o.

Table 4. Functional Dependence of Retention Indicator on Radius and Velocity for Each Pair of Controlling Solute Transfer and Freezing Processes[a]

Relevant Conditions			Adiabatic Freezing Control	Diabatic Freezing Control
Regime	Expression	Description		
		Gas-Phase Solute Transfer Control		
$\bar{F}_g$, $F_m \approx 1$	$[Sc_{wv\&sol}$ and $Pr]^{1/3}Re^{1/2} \lesssim 1$	low velocities, small drops	$\sim a$	–
$\bar{F}_g$, $F_m \gg 1$	$[Sc_{wv\&sol}$ and $Pr]^{1/3}Re^{1/2} \gtrsim 25$	high velocities, large drops	$\sim(a/u)^{1/2}$	–
		Interfacial Solute Transfer Control		
$\bar{F}_g \approx 1$	$[Sc_{wv\&sol}$ and $Pr]^{1/3}Re^{1/2} \lesssim 1$	low velocities, small drops	–	$\sim a^{-1}$
$\bar{F}_g \gg 1$	$[Sc_{wv\&sol}$ and $Pr]^{1/3}Re^{1/2} \gtrsim 25$	high velocities, large drops	–	$\sim(a/u)^{-1/2}$
		Aqueous-Phase Solute Transfer Control		
$\bar{F}_g$, $F_{aq} \approx 1$	$[Sc_{wv}$ and $Pr]^{1/3}Re^{1/2} \lesssim 1$, $(Re')^2Sc' \lesssim 900$	[b]	$\sim a$	–
$\bar{F}_g \gg 1$, $F_{aq} \approx 1$	$[Sc_{wv}$ and $Pr]^{1/3}Re^{1/2} \gtrsim 25$, $(Re')^2Sc' \lesssim 900$	[b]	$\sim a$	$\sim(au)^{1/2}$
$\bar{F}_g \gg 1$, $F_{aq} > 1$	$[Sc_{wv}$ and $Pr]^{1/3}Re^{1/2} \gtrsim 25$, $Re' \lesssim 3$	[b]	$\sim a^{-1}u^{-2}$	$\sim(au)^{-3/2}$
$\bar{F}_g \gg 1$, $F_{aq} \gg 1$	$[Sc_{wv}$ and $Pr]^{1/3}Re^{1/2} \gtrsim 25$, $Re' \gtrsim 3$	[b]	$\sim u^{-1}$	$\sim(au)^{-1 \text{ to } -1/2}$

[a]Conditions specified indicate general conditions for which the expression applies, if the given solute transfer process is controlling. Conditions under which each solute transfer process will be most important are given in Table 1. $Re' = Re(\mu_a/\mu_w)$, $Sc' = Sc(D_g/D_{aq})$.
[b]Velocity and drop size increase for each successive regime.

Table 6. Conditions and Freezing Times for the Typical Nonrime Freezing Case and Dry Growth Riming Without Spreading Case

	Drop Size, μm									
	1	5	10	25	50	100	250	500	1000	2000
Typical Nonrime Freezing										
Conditions										
T_∞, °C	−39	−34	−32	−29	−27	−25	−22	−20	−18	−16
P, mbar	300	300	300	300	300	300	300	300	300	300
pH	4.0	4.0	4.0	4.0	4.0	4.0	4.0	4.0	4.0	4.0
$u = v_t$, cm/s	0.02	0.4	1	8	30	90	300	600	1000	1500
Estimated freezing times										
τ_{f-ad}, s	4e-6	2e-5	5e-5	1e-4	3e-4	7e-4	2e-3	4e-3	9e-3	0.02
τ_{f-d}, s	4e-5	1e-3	5e-3	0.03	0.1	0.4	2	4	10	30
τ_{frz}, s	4e-5	1e-3	5e-3	0.03	0.1	0.4	2	4	10	30
Dry Growth Riming Without Spreading										
Conditions										
T_∞, °C	−10°C	−10°C	−10°C	−10°C	−10°C	−10°C	−10°C	−10°C	−10°C	−10°C
P, mbar	700	700	700	700	700	700	700	700	700	700
pH	4.0	4.0	4.0	4.0	4.0	4.0	4.0	4.0	4.0	4.0
u, cm/s	200	200	200	200	200	200	200	200	200	200
Estimated freezing times										
τ_{f-ad}, s	2e-5	1e-4	2e-4	5e-4	1e-3	2e-3	5e-3	0.01	0.02	0.04
τ_{f-d}, s	2e-4	5e-3	0.02	0.1	0.3	1	5	15	45	130
τ_{frz}, s	2e-4	5e-3	0.02	0.1	0.3	1	5	15	45	130

retention indicator increases directly with radius. For drops less than about 25 μm, interfacial transfer is also important (limiting for $a \approx 1$ μm) and the diabatic retention indicator decreases with radius. These trends are consistent with the functional dependencies specified in Table 4 for gas-phase and interfacial mass transfer control.

[33] For the nonrime freezing case, the gas-phase is similarly important. The diabatic retention indicator for drops larger than 25 μm decreases slightly with radius due to the increasing mean nucleation temperature and increasing terminal fall velocity. (For gas-phase control, retention is inversely related to both temperature and velocity, as shown in Tables 3 and 4, respectively.) For SO_2, the aqueous phase is also an important resistance to mass transfer for all drop sizes. Therefore, we see local maxima in the SO_2 retention indicators at intermediate radius (and velocity) as expected from Table 4 for aqueous-phase mass transfer control. The overall magnitude difference between the two cases is due mostly to the temperature differences between the cases.

[34] Results from our variability study indicate that the limiting mass transfer regime depends very significantly on solute properties. Specifically, the effective Henry's constant, aqueous-phase solute diffusivity, and the accommodation coefficient are important. Table 1 provides expressions and a summary describing how these properties interact to determine the limiting mass transfer regime. Table 2 lists the derived dependence of the retention indicator on solute properties for each controlling mass transfer regime. The retention indicator varies inversely with gas-phase diffusivity, accommodation coefficient, and aqueous-phase diffusivity if the relevant mass transfer regime is important. If gas-phase or interfacial mass transfer are important, the retention indicator varies directly with the effective Henry's constant.

[35] The Henry's constant varies widely between chemicals. For relatively soluble species or semi-soluble species that dissociate significantly, the gas phase limits mass transfer for all but the smallest drop sizes, and the retention indicators are generally much greater than one. We found this to be true for $K_H^* (= \beta K_H) \gtrsim 1 \times 10^4$M/atm for F_{aq} and $F_m \approx 1$ (and typical values of D_{aq} and α). For increasing velocities and sizes this cut-off value increases. For very volatile species and species that do not dissociate, the aqueous phase limits mass transfer, generally resulting in much lower retention indicators.

[36] Aqueous-phase diffusivities do not vary significantly between chemicals or conditions, and hence would likely only have a very small effect on retention if only this variability were important. However, we use D_{aq} to represent the diffusivity in the condensed-phase, which can include diffusivity through and ice shell with water fissures. Diffusivities in such a system are not well characterized. Hence, in our variability study we examined D_{aq} values from those representative of aqueous-phase transfer ($\approx 1 \times 10^{-5}$ cm^2/s) to values more representative of ice-phase transfer ($\approx 1 \times 10^{-12}$ to 1×10^{-10} cm^2/s). Smaller values of D_{aq} cause the condensed-phase to be a more important resistance to the solute transfer. For the conditions of our dry growth riming case with D_{aq} varied, the condensed phase dominates mass transfer for SO_2, H_2O_2, and NH_3 at $D_{aq} \lesssim 5 \times 10^{-7}$, 1×10^{-9}, and 1×10^{-11} cm^2/s, respectively. Figure 3a shows the retention indicators for $D_{aq} = 1 \times 10^{-9}$ cm^2/s. With decreased D_{aq}, the overall magnitude of the SO_2 retention indicator increases, indicating increased retention if an ice shell significantly impedes mass transfer. We also see that the dependence of the H_2O_2 and SO_2 retention indicators on radius are very similar in Figure 3 due to the condensed-phase mass transport limitation.

[37] For the chemicals studied here, the mass accommodation coefficient is on the order of 0.1 at T_o. For chemicals or conditions that result in significantly lower mass accommodation coefficients, interfacial transfer is important. For $\alpha \lesssim 1 \times 10^{-2}$, the retention indicator

Table 7. Solute Mass Transfer Timescales and Retention Indicators for the Typical Nonrime Freezing Case[a]

	Drop Size, μm									
	1	5	10	25	50	100	250	500	1000	2000
Sulfur Dioxide, H = 1.8e4*										
Solute mass transfer timescales, s										
τ_g, s	2e-4	5e-3	2e-2	1e-1	4e-1	1	4	9	20	50
τ_i, s	8e-4	4e-3	8e-3	2e-2	4e-2	8e-2	2e-1	4e-1	7e-1	1
τ_{aq}, s	1e-4	3e-3	1e-2	8e-2	3e-1	1	5	2	1	2
τ_{exp}, s	6e-3	1e-2	4e-2	2e-1	8e-1	3	9	10	20	50
Limiting resistance	i	g	g	g	g	g	aq	aq	G	G
Retention indicator										
τ_{exp}/τ_{f-ad}	300	500	800	2000	3000	4000	5000	3000	3000	3000
τ_{exp}/τ_{f-tot}	30	10	8	7	6	6	5	3	2	2
Hydrogen Peroxide, H = 1.5e7*										
Solute mass transfer timescales, s										
τ_g, s	1e-1	3	20	70	200	700	3000	6000	1e4	3e4
τ_i, s	2-1	1	2	6	10	20	60	100	200	400
τ_{aq}, s	9e-5	2e-3	9e-3	6e-2	2e-1	9e-1	4	2	1	2
τ_{exp}, s	3e-1	4	10	70	300	800	3000	6000	1e4	3e4
Limiting resistance	i	g	g	G	G	G	G	G	G	G
Retention indicator										
τ_{exp}/τ_{f-ad}	8e4	2e5	3e5	5e5	8e5	1e6	1e6	1e6	2e6	2e6
τ_{exp}/τ_{f-tot}	8000	4000	3000	2000	2000	2000	2000	1000	1000	1000
Ammonia, H = 1.7e9*										
Solute mass transfer timescales, s										
τ_g, s	10	200	900	6000	2e4	7e4	2e5	5e5	1e6	3e6
τ_i, s	40	200	400	1000	2000	4000	1e4	2e4	4e4	8e4
τ_{aq}, s	9e-5	2e-3	9e-3	6e-2	2e-1	9e-1	4	2	1	2
τ_{exp}, s	50	500	1000	7000	2e4	7e4	2e5	6e5	1e6	3e6
Limiting resistance	i	g	g	g	G	G	G	G	G	G
Retention indicator										
τ_{exp}/τ_{f-ad}	1e7	2e7	3e7	5e7	8e7	1e8	1e8	1e8	1e8	2e8
τ_{exp}/τ_{f-tot}	1e6	4e5	3e5	2e5	2e5	2e5	1e5	1e5	1e5	1e5
Nitric Acid, H = 1.0e13*										
Solute mass transfer timescales, s										
τ_g, s	1e5	3e6	1e7	7e7	2e8	7e8	2e9	5e9	1e10	3e10
τ_i, s	3e5	2e6	3e6	8e6	2e7	3e7	8e7	2e8	3e8	6e8
τ_{aq}, s	1e-4	3e-3	1e-2	8e-2	3e-1	1	5	2	1	2
τ_{exp}, s	4e5	4e6	1e7	8e7	7e8	7e8	2e9	5e9	1e10	3e10
Limiting resistance	i	g	g	g	G	G	G	G	G	G
Retention indicator										
τ_{exp}/τ_{f-ad}	1e11	2e11	3e11	5e11	9e11	1e12	1e12	1e12	1e12	1e12
τ_{exp}/τ_{f-tot}	1e10	4e9	3e9	2e9	2e9	2e9	1e9	1e9	1e9	1e9

[a]Only orders of magnitude are shown, but calculations are made with the precise numbers. For the limiting resistance, 'AQ' is for aqueous-phase, 'I' is for interfacial, and 'G' is for gas-phase. Uppercase signifies that the resistance controls mass transfer (the timescale is more than 10× greater than both of the other timescales). Lowercase signifies that resistance has the longest timescale, but other resistances are also important.

Table 8. Variable Values Considered for the Variability Study and the General Impacts of Varying Each Parameter on Retention Indicator

Parameter Varied	Range Considered	General Impacts on Retention Indicator
		Solute Properties
Effective Henry's constant H^*	1e-3 to 1e22	Very large effects. Controls limiting regime. Directly related if gas-phase or interfacial control.
Condensed-phase diffusivity D_{aq}, cm^2/s	1e-12 to 1e-5	Large effects. Affects limiting regime. Inversely related for small drops and low velocities if condensed-phase control. Significant effects.
Accommodation coefficient α	1e-4 to 1	Affects limiting regime. Inversely related, if interfacial control.
Gas-phase diffusivity D_g, cm^2/s	0.01 to 1	Small effects. Inversely related if gas-phase control.
		Conditions
pH	1 to 13	Very large effects if dissociation potential. Affects H^* and limiting regime. Dependence is chemical specific.
Temperature T_∞, °C	−39 to −1	Large effects, inversely related. τ_{exp}/τ_{f-ad} and τ_{exp}/τ_{f-tot} vary by 3 and 2 orders of magnitude, respectively, over the temperature range studied.
Drop size a, μm	1 to 2000	Significant effects, nonmonotonic dependence. τ_{exp}/τ_{f-ad} and τ_{exp}/τ_{f-tot} vary by ≲3 and 1 orders of magnitude, respectively, over the size range studied.
Drop velocity u, cm/s	0.01 to 5000	Significant effects, nonmonotonic dependence. τ_{exp}/τ_{f-ad} and τ_{exp}/τ_{f-tot} vary by ≲ 2 and 1 orders of magnitude, respectively, over the velocity range studied.
Pressure P, mbar	100 to 1013	Small effects. τ_{exp}/τ_{f-ad} and τ_{exp}/τ_{f-tot} vary by ≲5×

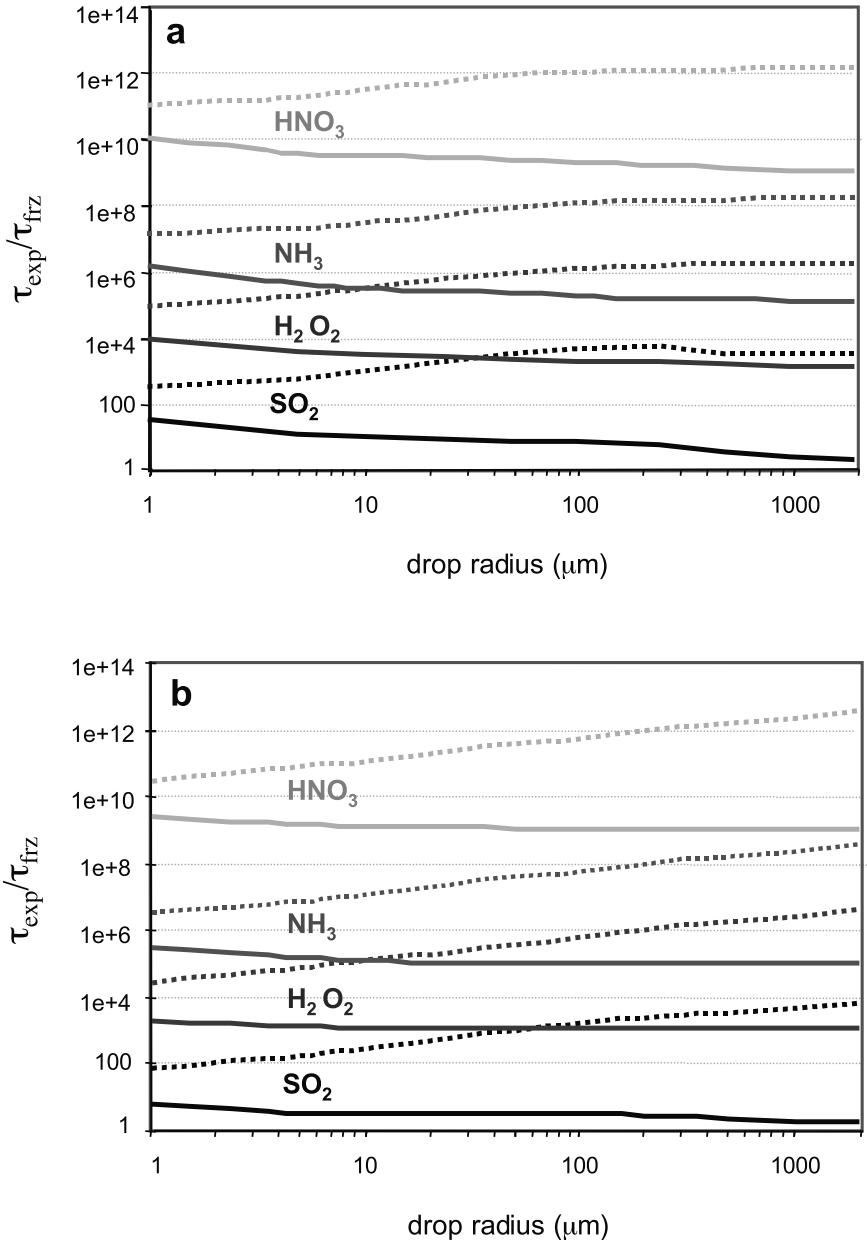

Figure 2. Retention indicator versus radius for the nonrime freezing case (a) and dry growth riming without spreading case (b) for SO_2 (black), H_2O_2 (dark gray), NH_3 (medium gray), and HNO_3 (light gray). The dotted lines are for adiabatic freezing (impermeable ice shell formation) and the solid lines are for total drop freezing. Note that all scales are logarithmic.

depends significantly on α. For higher α (including values relevant for the chemicals studied here), α is important for small drop sizes ($a \lesssim 25$ μm) and has little impact for larger drops. For $\alpha \lesssim 1 \times 10^{-3}$ interfacial mass transfer is the dominant resistance. Figure 3b shows the retention indicator for the dry growth riming case with $\alpha = 1 \times 10^{-3}$. For lower α, the overall magnitude of the adiabatic retention indicator for all species is significantly increased. This is also true for the diabatic retention indicator except for the largest drops. For interfacial mass transfer control, the adiabatic retention indicator is not a function of drop size and the total retention indicator decreases with drop size, as specified in Table 4.

[38] Gas-phase diffusivities do not vary significantly between chemicals, but they do vary with pressure. Gas-phase diffusivities vary by about an order of magnitude over the pressure range studied here. If the gas-phase limits mass transfer, higher pressures result in lower D_g, which has a small inverse effect on the retention indicators.

[39] For any given chemical (i.e., set of solute properties), the retention indicator will depend on the conditions of freezing. Since the limiting regime and magnitude of the retention indicator depend so significantly on the effective Henry's constant, the pH is the most important condition variable for chemicals which dissociate. Figure 4 shows the variation in retention indicator with pH for the four chem-

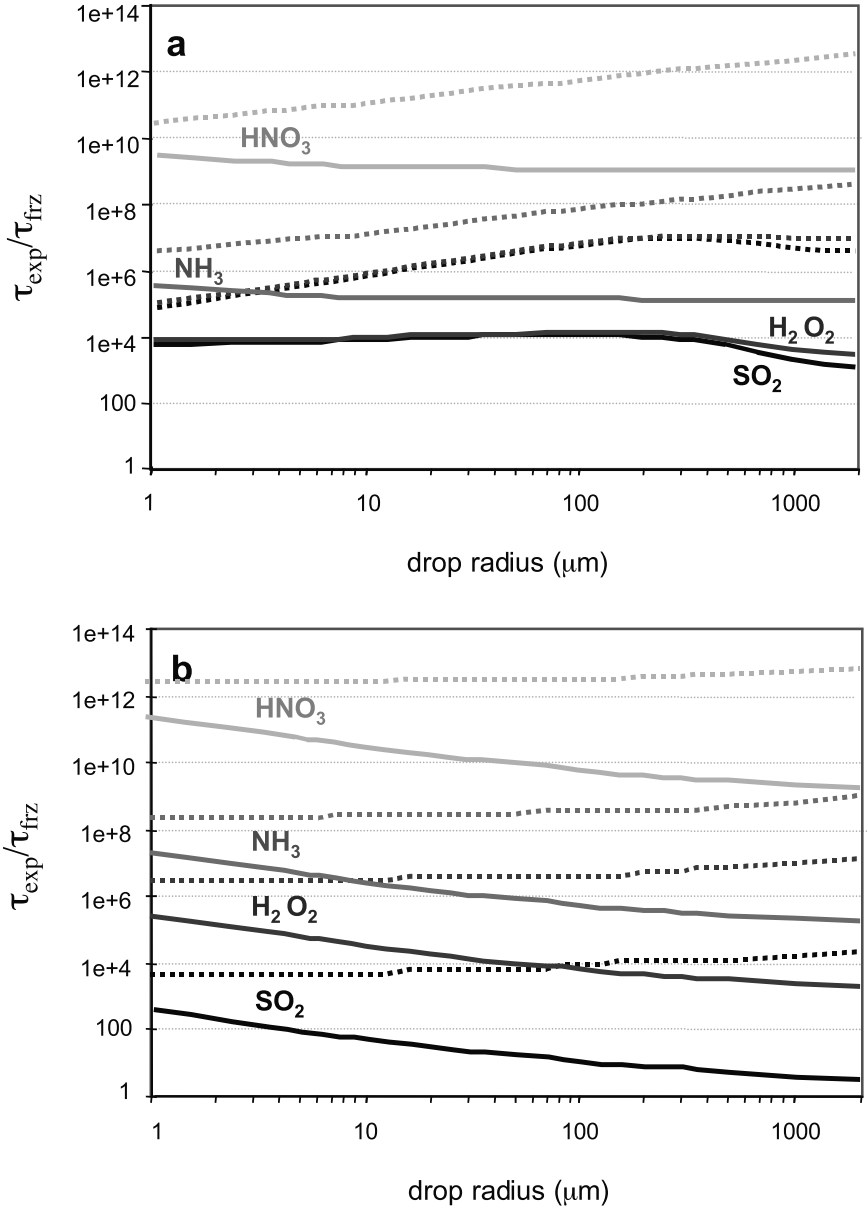

Figure 3. Retention indicator versus radius for condensed-phase diffusivity, D_{aq}, of 1×10^{-9} cm^2/s (a) and mass accommodation coefficient, α, of 1×10^{-3} (b) for SO_2 (black), H_2O_2 (dark gray), NH_3 (medium gray), and HNO_3 (light gray). All other conditions are those of the dry growth riming without spreading case. The dotted lines are for adiabatic freezing and the solid lines are for total drop freezing.

icals studied. Values were calculated for the conditions of the dry growth riming case with pH varied independently. For SO_2 we see a direct dependence of retention indicator on pH. For low pH ($\lesssim$3) the aqueous phase limits solute transfer and the total (diabatic) retention indicator is on the order of one. For NH_3, the retention indicator is inversely related to pH. For high pH ($\gtrsim$9) the total (diabatic) retention indicator is on the order of one. (The aqueous phase limits transfer for pH $\gtrsim$ 10.) For these conditions we would expect significant loss during freezing of sulfur dioxide at pH $\lesssim$ 3 and ammonia at pH $\gtrsim$ 9, if a complete ice shell does not form or significantly impede solute transport. For HNO_3, the dependence on pH is direct. However, the effective Henry's constant is so high under all reasonable pH conditions that we would expect complete retention. For H_2O_2 there is no dependence on pH as it does not dissociate significantly.

[40] Along with pH, the retention indicator also varies with temperature, drop size, velocity, and pressure. The variance with these conditions is significantly less than the variance with pH for dissociating chemicals. However, for chemicals in systems with the combination of solute properties and pH that results in retention indicators on the order of one, these variables likely determine the degree of retention. Figure 5 shows the variance of the SO_2 retention indicator with each of these variables at pH = 3. Tables 3 and 4 provide the derived functional dependencies. Figures 5a and 5b show the direct, mon-

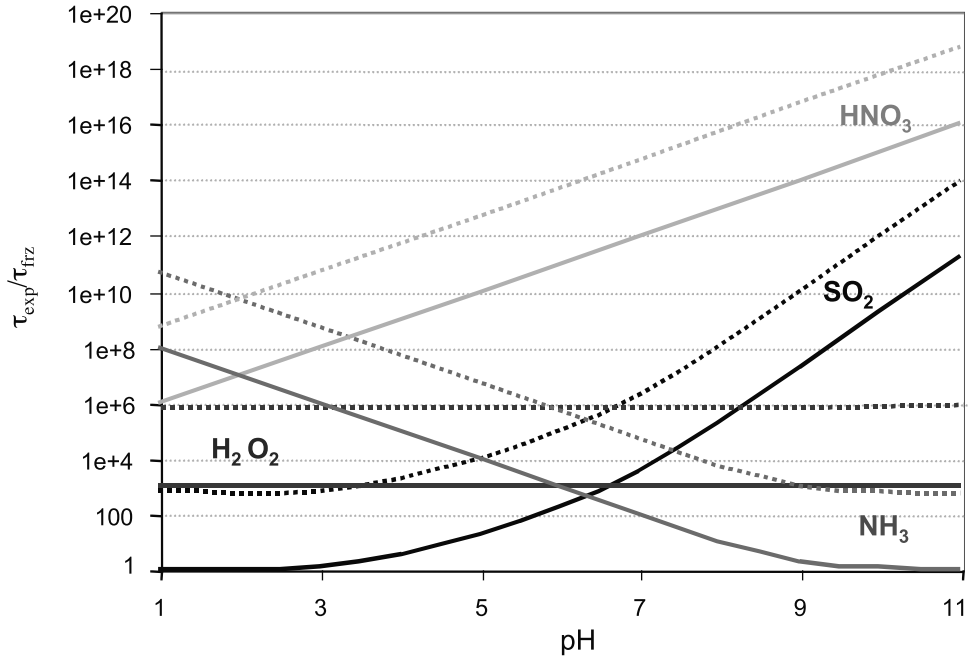

Figure 4. Dependence of retention indicator on pH for SO_2 (black), H_2O_2 (dark gray), NH_3 (medium gray), and HNO_3 (light gray) for a 100 μm drop. (The form of the dependence is not a function of radius). Conditions are those of the dry growth riming case with pH varied independently. The dotted lines are for adiabatic freezing and the solid lines are for total drop freezing.

otonic dependence of retention indicator on the supercooled delta temperature of the drop (i.e., inverse dependence on air/drop temperature). Figures 5c and 5d and Figures 5e and 5f show the nonmonotonic dependence of the retention indicators on radius and velocity, respectively. The total retention indicator exhibits a maximum at intermediate values of $au(\approx 1\ cm^2/s)$, due to the competing effects of ventilation enhancement on heat and mass transfer. Figures 5g and 5h show that pressure has very small effects for pressures greater than about 400 mbar, for condensed-phase mass transfer control. For lower pressures the total retention indicator and adiabatic retention indicator (for the largest drop sizes) decrease with increasing pressure.

[41] Finally, we see from all the graphs that the adiabatic retention indicator is one to three plus orders of magnitude greater than the total freezing (diabatic) retention indicator (the difference increases with radius). Therefore we would expect retention to be much greater (close to complete under most conditions) if an impermeable ice shell forms soon after the adiabatic stage. If no shell forms or does not significantly impede solute transfer (D_{aq} for water), there may be significant loss during freezing.

7. Comparison With Laboratory Data

[42] In this paper, we have focused on conditions of nonrime freezing and dry growth riming with minimal spreading because they provide a significant first step towards understanding the retention phenomena and developing a methodology for predicting it, and they are specifically relevant to an understudied solute retention process in clouds (nonrime freezing). Since available experimental data on retention are for conditions of mixed dry and wet growth riming, we focus on qualitatively comparing our predicted retention indicator dependence to the experimental retention coefficient dependence.

7.1. Effect of Chemical Volatility/Solubility

[43] There are eight experimental studies [*Iribarne et al.*, 1983, 1990; *Lamb and Blumenstein*, 1987; *Iribarne and Pyshnov*, 1990; *Snider et al.*, 1992; *Iribarne and Barrie*, 1995; *Snider and Huang*, 1998; *Voisin et al.*, 2000] which have measured retention during drop freezing for the following chemicals: SO_2, H_2O_2, NH_3, HNO_3, HCl, O_2, HCOOH, and CH_3COOH. Conditions of pH, temperature, pressure, ventilation, and drop size varied between and within studies. For some studies, information about each of these parameters is not available. All studies for which pH was measured were done at relatively low pH (though the range included between about 2.4 and 7.5). Temperatures varied between −1 and −24 °C, pressures varied between about 1013 and 670 mbar, velocities varied between 2×10^{-3} and 2400 cm/s, and drop size varied between about 2 μm and 5 mm. To qualitatively compare our chemical specific results with the experimental data, we have calculate the effective Henry's constant (H^*) for each of these chemicals as for the dry growth rime without spreading case (at pH = 4 and T_o). Table 9 lists the chemicals, H^*, the average adiabatic and total retention indicators for chemicals considered in our dry growth riming without spreading case, and the range of experiment retention data. Chemicals are presented in order of increasing effective Henry's constant. The table shows that the experimental retention indicators map relatively well with the calculated effective Henry's

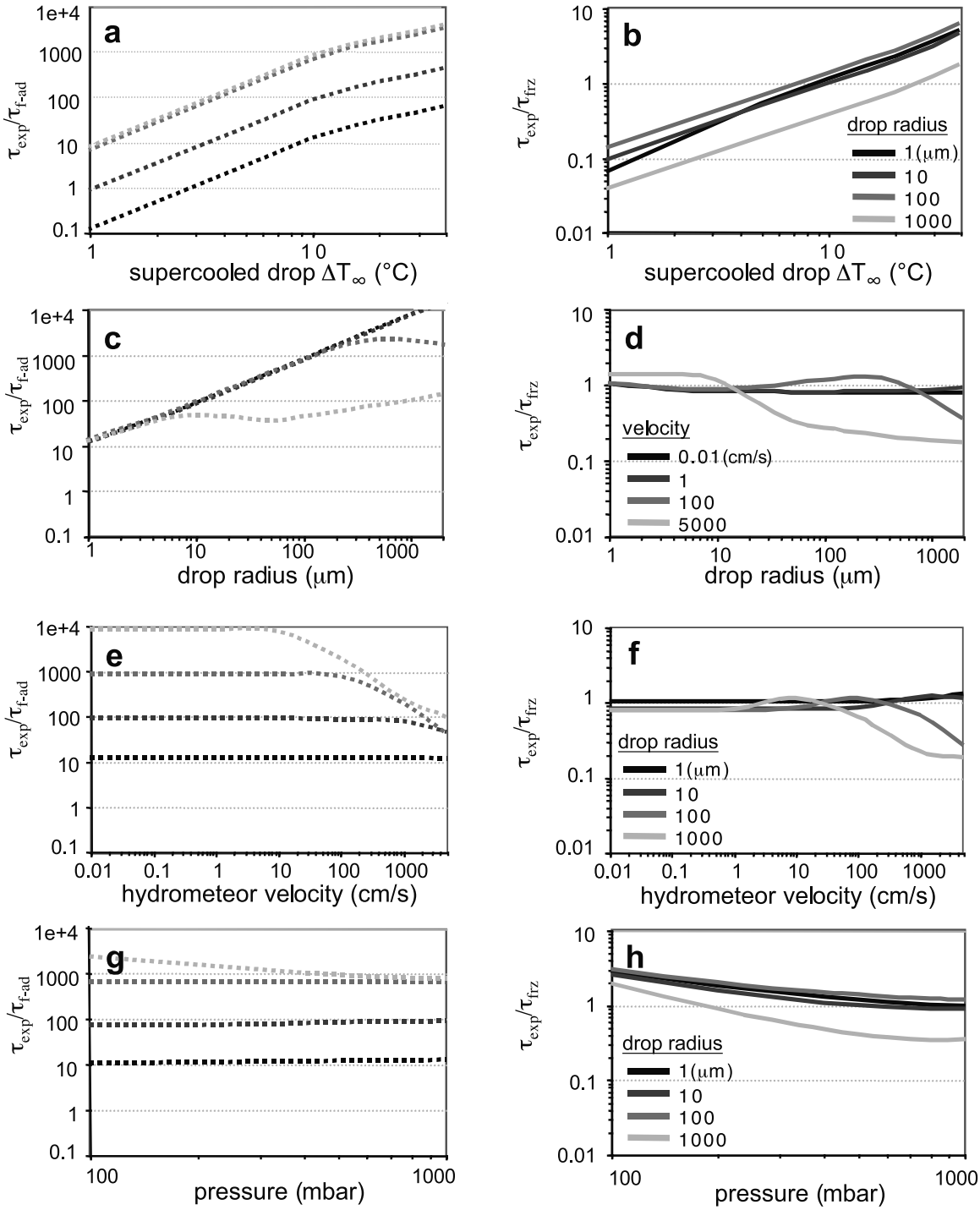

Figure 5. Dependence of the SO_2 retention indicator on independent changes in temperature (a, b), drop radius (c, d), hydrometeor velocity (e, f), and pressure (g, h). The left hand column is for adiabatic freezing (dotted lines) and the right hand column is for total drop freezing (note that the scales are different).

constant and retention indicators. Chemicals who were consistently measured as experiencing complete retention (HCl, HNO_3, NH_3) have the highest effective Henry's constants and calculated retention indicators. Chemicals with lower effective Henry's constants and retention indicators have a broad range of measured retention, indicating that specific freezing conditions, rather than chemical solubility/volatility, may play a significant role in determining retention.

7.2. Effect of pH

[44] A few experimental studies [*Iribarne et al.*, 1990; *Snider et al.*, 1992; *Iribarne and Barrie*, 1995; *Sato et al.*, 1996] have considered the effect of pH on retention. All but

Table 9. Comparison of Effective Henry's Constants and Calculated Retention Indicators (Average Values) to Measured Retention Data[a]

Chemical	H^*	τ_{exp}/τ_{f-tot}, τ_{exp}/τ_{f-ad}	Measured Retention Fraction
O_2	2.9×10^{-2}	–	0.17 to 0.52
SO_2	1.8×10^{4}	3, 2×10^{3}	0.01 to 0.83
HCOOH	1.4×10^{6}	–	>0.5
CH_3COOH	1.6×10^{6}	–	>0.5
H_2O_2	1.5×10^{7}	1×10^{3}, 9×10^{5}	0.01 to 1
NH_3	1.7×10^{9}	1×10^{5}, 9×10^{7}	1
HNO_3	1.0×10^{13}	1×10^{9}, 8×10^{11}	1
HCl	4.4×10^{15}	–	1

[a]A dash signifies that retention indicators for this chemical were not calculated in this study.

one of these studies found a dependence of retention on pH. *Iribarne et al.* [1990] found no dependence, but they only considered a very small pH range. The studies which found a pH dependence propose that this dependence is due to reactivity. Our results indicate the pH will have a significant impact on the effective Henry's constant, mass transfer times, and retention. Due to the limited nature of the experimental data regarding pH, this result is neither refuted nor corroborated by the data.

7.3. Effect of Temperature

[45] A few experimental studies of riming retention found retention to be approximately directly linearly related to the supercooling delta temperature, ΔT_∞, although with different slopes and intercepts [*Lamb and Blumenstein*, 1987; *Iribarne et al.*, 1990; *Snider et al.*, 1992]. Our development (summarized in Table 3) leads to a direct functional dependence of retention indicator on ΔT_∞ for both adiabatic and diabatic freezing control. For adiabatic control, we predict the dependence to be on ${\Delta T_\infty}^2$ and ΔT_∞, for $T > -10°C$ and $T < -10°C$, respectively. For diabatic freezing control at temperatures greater than approximately $-20°C$, we predict a dependence on ΔT_∞. Since experimental conditions for the above studies included temperatures between -2 and $-24°C$, our results are consistent with the experimental data.

7.4. Effect of Drop Size

[46] *Lamb and Blumenstein* [1987] found retention coefficients for SO_2 to be approximately an order of magnitude smaller than those found by *Iribarne et al.* [1990], under somewhat similar ventilation and temperature conditions. However, the drop sizes observed by each research group were somewhat different. Lamb and Blumenstein observed small drops ≤ 10 μm in radius, while Iribarne et al. observed drops ranging from 5 to 40 μm in radius, with a mass-weighted mean radius of 28.5 μm. Iribarne et al. suggested that the radius difference between the studies could not account for the differences in retention. Based on a qualitative discussion of expected effects of radius on ice growth rates, he speculated that the dependence of retention on radius should be inverse. Our analysis, which includes the completing effect of radius on freezing and mass transfer rates, indicates that for aqueous-phase limited solute transfer and diabatic freezing control, retention varies directly with radius for smaller drops and velocities ($au \lesssim 1$ cm^2/s, Figure 5d), and inversely with radius, as Iribarne et al. suggested, for larger drops and velocities. This result is consistent with the experimental observations.

7.5. Effect of Ventilation

[47] Ventilation conditions in the experimental studies varied significantly and trends based on comparison of experimental studies are not readily apparent. However, in one study of SO_2 retention during riming, *Iribarne et al.* [1990] investigated retention under three distinct freezing and ventilation conditions: (1) gravitational collection (fall velocities ≈10 cm/s), (2) collection on rotating rods (air velocities about an order of magnitude higher), and (3) jet experiments (air velocities several times higher than the second case). They found retention to increase from case 1 to case 2 and then to slightly decrease from case 2 to case 3. Our analysis provides a possible explanation for this trend. The trend may be due to the competing effects of ventilation on diabatic freezing time and solute expulsion time for aqueous-phase limited transfer. We predict a direct relationship between retention and velocity for lower velocities, and an inverse relationship at higher velocities (see Figure 5f and Table 4), consistent with Iribarne's observations.

8. Limitations

[48] Although our development is a significant step toward understanding the retention phenomena, it necessarily simplifies the complexity of the process interactions involved. Here, we discuss these limitations and their implications.

8.1. Physical Processes

[49] Several physical processes were not explicitly considered here that are likely to be important in clouds under certain conditions. These include spreading of drops on impact with the rimer, heat transfer to the riming substrate, loss of solutes from frozen ice, and several processes involved in wet growth riming.

[50] At higher temperatures of the ice substrate, impact speeds, and drop sizes, drops spread to a greater degree during riming [*Macklin and Payne*, 1969]. Spreading of drops would effectively decrease the diffusion length in this analysis and hence the expulsion time. It would also provide more surface area for heat transfer to the ice substrate, decreasing the freezing time.

[51] The diabatic freezing time equation used here does not consider heat transfer to the underlying ice substrate. Using an iterative model to calculate heat loss [after *Baker et al.*, 1987] and accounting for spreading, we found that the freezing time decreased by about 15 to 90% when heat loss to the substrate was included, under the conditions of the *Lamb and Blumenstein* [1987] and *Iribarne et al.* [1990] experimental studies.

[52] After freezing, solutes in the ice hydrometeor can be lost to air through diffusion in the crystal structure, at crystal grain boundaries, or in cracks formed during freezing. Diffusivities of chemicals in solid ice are orders of magnitude less than those in water [e.g., *Sommerfeld et al.*, 1998; *Thibert and Dominé*, 1998]. If the solute diffusivity in frozen ice is in the upper range of measured values (≈1 $\times 10^{-10}$ cm^2/s), loss after freezing may be significant only for the smallest drop sizes (≈1 μm).

[53] Freezing during wet growth is significantly different from nonrime freezing and dry growth riming. Different processes are important, including coalescence of several drops in an unfrozen layer prior to freezing, burial of partially frozen drops by newly collected drops, and shedding of water. The analysis provided here is not applicable to wet growth riming.

8.2. Chemical Processes

[54] In addition to physical processes, there are chemical processes occurring during freezing. These include chemical dissociation/association in water and aqueous-phase and ice-surface reactions.

[55] Our analysis assumes that the association processes are fast compared with the other mass transfer and freezing timescales. This is a good assumption for the chemicals considered. If the association processes are slow, the chemical's volatility would effectively be decreased, increasing the Henry's constant and the retention indicator values.

[56] Reaction processes will affect the solute diffusivities in water and air, the solute volatility and solubility in water (Henry's constant), and the solute solubility in ice. Our variability study indicates that the retention indicator depends on the solute diffusivities. However, diffusivities do not vary much between species, so chemical reactions are not likely to impact retention significantly through changed diffusivities. Conversely our analysis indicates that changes in the Henry's constant will significantly impact retention. Changes in the ice-water partition coefficient could impact the concentration of solute in the aqueous phase, which drives mass transfer. However, for dendritic growth where trapping predominates, equilibrium ice-water partitioning is likely not very important.

9. Summary and Conclusions

[57] In this paper, we developed a scaling methodology for examining retention of volatile chemicals during freezing of cloud hydrometeors. Using this methodology, we developed a theory-based indicator of retention from which we determined the likely dependence of retention on important solute properties and freezing conditions. The development in this paper is valid for nonrime freezing conditions and for dry growth riming conditions for which drop spreading on contact is minimal. The results are also somewhat applicable to riming with spreading, as many of the phenomena involved are similar. Our conclusions are as follows:

1. Retention is likely very chemical specific, as it is highly dependent on the effective Henry's constant. Chemicals with high effective Henry's constants (e.g., HNO_3) are likely to be retained completely under all nonrime freezing and dry growth riming conditions. Retention likely decreases with decreasing effective Henry's constant.

2. For chemicals with low enough effective Henry's constants for measurable loss during freezing (e.g., SO_2, H_2O_2), retention is likely much greater when a complete ice shell forms soon after the adiabatic freezing stage than when no shell forms. If a partial ice shell or ice-shell with water fissures forms, retention could also be significantly increased.

3. For chemicals that dissociate significantly in water (e.g., SO_2 and NH_3), retention is likely very dependent on pH. The dependence on pH is chemical specific; SO_2 is likely retained more at high pH while NH_3 is lost more at high pH.

4. For chemicals with low enough effective Henry's constants for measurable loss during freezing, variations in temperature, drop size, and the magnitude of the hydrometeor velocity likely have significant impacts on retention. Retention is not very pressure dependent.

5. Retention increases with decreasing temperature. The variation of retention with hydrometeor velocity and drop size is dependent on the limiting solute mass transfer regime. For more soluble chemicals (intermediate K^*_H, e.g., H_2O_2), most drop sizes, and condensed-phase solute transfer that is not significantly impeded by ice, the gas-phase is most limiting. If an ice shell forms immediately after the adiabatic stage, retention increases with radius and decreases with velocity. If no shell forms, retention is independent of radius and velocity. For very small drops ($a \lesssim 1$ μm) or for chemicals with very small accommodation coefficients ($\alpha \lesssim 1 \times 10^{-3}$), the interface limits solute transfer. Retention then increases with velocity and decreases with radius if no ice shell forms. For very volatile chemicals, (e.g., SO_2 at a pH of 3), or conditions were condensed-phase solute transfer is impeded by ice, the condensed-phase limits solute transfer. Retention is then likely to be maximized at intermediate drop sizes and velocities.

[58] This work provides hypotheses to test in new experiments on retention, conditions that are likely important to control (or quantify) in new laboratory and field studies, and dependence functions that can be used to develop parameterizations of retention for cloud modeling.

Notation

a	supercooled drop radius, cm or μm.
c'	high temperature constant for adiabatic freezing, cm/s/°C.
c''	low temperature constant for adiabatic freezing, cm/s/°C.
c_w	heat capacity of water at constant pressure, cal/g/°C.
D_{aq}	diffusivity of solute in the condensed (aqueous) phase, cm^2/s.
D_v	diffusivity of water vapor in air, cm^2/s.
D_g	diffusivity of solute in air, cm^2/s.
F_{aq}	aqueous-phase ventilation coefficient.
F_g	gas-phase ventilation coefficient (general term).
$\bar{F}_g$	average gas-phase vent. coefficient (heat and water vapor).
F_m	gas-phase solute transfer ventilation coefficient.
G	intrinsic growth rate of ice in supercooled water, cm/s.
H^*	effective concentration Henry's constant, unitless.
K_H	Henry's constant, M/atm.
K^*_H	effective Henry's constant, M/atm.
k_a	thermal conductivity of air, cal/cm/s/°C.
L_m	latent heat of water melting, cal/g.

L_s latent heat of water sublimation, cal/g.
m exponential constant in adiabatic retention indicator equation.
P Pressure, mbar.
Pr gas-phase Prandtl number.
R universal gas constant, L atm/mol K.
Re Reynolds number.
Re' modified Re for circulation in drops.
Sc gas-phase Schmidt number (wv for water vapor, sol for solute).
Sc' modified Schmidt number for transfer in drops.
T_o equilibrium freezing temperature of water, °C.
T_∞ air and supercooled drop temperature, °C.
ΔT_∞ $T_o - T_\infty$, °C.
u drop velocity in air, cm/s.
$\bar{v}$ thermal velocity, cm/s.
v_t drop terminal fall velocity, cm/s.
α interfacial accommodation coefficient.
β dissociation factor.
η_a dynamic viscosity of air, g/cm/s.
η_w dynamic viscosity of water, g/cm/s.
ρ_w density of the water drop, g/cm^3.
$\overline{\left(\frac{d\rho v}{dT}\right)}_{\mathrm{sat,i}}$ mean slope of vapor saturation density curve over ice, g/cm^3/°C.
τ_{aq} condensed (aqueous)-phase solute transfer timescale, sec.
τ_{exp} overall solute expulsion timescale, sec.
τ_{f-ad} adiabatic freezing time, sec.
τ_{f-d} diabatic freezing time, sec.
τ_{frz} total freezing time, sec.
τ_g gas-phase solute mass transfer timescale, sec.
τ_i interfacial solute transfer timescale, sec.
τ_{exp}/τ_{f-ad} adiabatic freezing time retention indicator.
τ_{exp}/τ_{f-tot} total freezing time retention indicator.
τ_{exp}/τ_{frz} retention indicator (general term).

[59] **Acknowledgments.** This work was supported by a U.S. Environmental Protection Agency STAR Graduate Fellowship (U915641). Partial support was also provided through grants from the National Science Foundation (grants ATM9694118 and ATM0101596) and the National Aeronautics and Space Administration (grant NAG5-8645). We would like to thank Jeff Cunningham, Frank Freedman, and Mary Barth for helpful comments on the manuscript.

References

Audiffren, N., S. Cautenet, and N. Chaumerliac, A modeling study of the influence of ice scavenging on the chemical composition of liquid-phase precipitation of a cumulonimbus cloud, *J. Appl. Meteorol.*, *38*, 1148–1160, 1999.

Baker, B., M. B. Baker, E. R. Jayaratne, J. Latham, and C. P. R. Saunders, The influence of diffusional growth rates on the charge transfer accompanying rebounding collisions between ice crystals and soft hailstones, *Q. J. R. Meteorol. Soc.*, *113*, 1193–1215, 1987.

Baker, R. A., Trace organic contaminant concentration by freezing, I, Low inorganic aqueous solutions, *Water Res.*, *1*, 61–77, 1967.

Barth, M. C., A. L. Stuart, and W. C. Skamarock, Numerical simulations of the July 10, 1996, Stratospheric-Tropospheric Experiment: Radiation, Aerosols, and Ozone (STERAO)–Deep Convection experiment storm: Redistribution of soluble tracers, *J. Geophys. Res.*, *106*(D12), 12,381–12,400, 2001.

Bertram, A. K., T. Koop, L. T. Molina, and M. J. Molina, Ice formation in $(NH_4)_2SO_4$-H_2O particles, *J. Phys. Chem. A*, *104*, 584–588, 2000.

Borys, R. D., P. J. Demott, E. E. Hindman, and D. Feng, The significance of snow crystal and mountain-surface riming to the removal of atmospheric trace constituents from cold clouds, in *Precipitation Scavenging, Dry Deposition, and Resuspension: Proceedings of the Fourth International Conference*, pp. 181–189, Elsevier Sci., New York, 1982.

Chen, J.-P., and D. Lamb, The role of precipitation microphysics in the selective filtration of air entering the upper troposphere, paper presented at 1990 Conference on Cloud Physics, Am. Meteorol. Soc., San Francisco, Calif., 1990.

Cho, H. R., M. Niewiadomski, and J. Iribarne, A model of the effect of cumulus clouds on the redistribution and transformation of pollutants, *J. Geophys. Res.*, *94*(D10), 12,895–12,910, 1989.

Clapp, L. M., R. F. Niedziela, L. J. Richwine, T. Dransfield, R. E. Miller, and D. R. Worsnop, Infrared spectroscopy of sulfuric acid water aerosols: Freezing characteristics, *J. Geophys. Res.*, *102*(D7), 8899–8907, 1997.

Davidovits, P., J. H. Hu, D. R. Worsnop, M. S. Zahniser, and C. E. Kolb, Entry of gas molecules into liquids, *Faraday Discuss.*, *100*, 65–82, 1995.

Edie, D. D., and D. J. Kirwan, Impurity trapping during crystallization from melts, *Ind. Eng. Chem. Fundam.*, *12*(1), 100–106, 1973.

Griggs, D. J., and T. W. Choularton, Freezing modes of riming droplets with application to ice splinter production, *Q. J. R. Meteorol. Soc.*, *109*, 243–253, 1983.

Gross, G. W., P. M. Wong, and K. Humes, Concentration dependent solute redistribution at the ice-water phase boundary, III, Spontaneous convection, chloride solutions, *J. Chem. Phys.*, *67*, 5264–5274, 1977.

Harrison, J. D., and W. A. Tiller, Controlled freezing of water, in *Ice and Snow: Properties, Processes, and Applications*, edited by W. D. Kingery, pp. 215–225, MIT Press, Cambridge, Mass., 1963.

Hobbs, P. V., *Ice Physics*, Clarendon, Oxford, England, 1974.

Iribarne, J. V., and L. A. Barrie, The oxidation of S(IV) during riming by cloud droplets, *J. Atmos. Chem.*, *21*, 97–114, 1995.

Iribarne, J. V., and T. Pyshnov, The effect of freezing on the composition of supercooled droplets, I, Retention of HCl, HNO3, NH3, and H2O2, *Atmos. Environ., Part A*, *24*(2), 383–387, 1990.

Iribarne, J. V., L. A. Barrie, and A. Iribarne, Effect of freezing on sulfur dioxide dissolved in supercooled droplets, *Atmos. Environ.*, *17*(5), 1047–1050, 1983.

Iribarne, J. V., T. Pyshnov, and B. Naik, The effect of freezing on the composition of supercooled droplets, II, Retention of S(IV), *Atmos. Environ., Part A*, *24*(2), 389–398, 1990.

Lamb, D., and R. Blumenstein, Measurement of the entrapment of sulfur dioxide by rime ice, *Atmos. Environ.*, *21*(8), 1765–1772, 1987.

Macklin, W. C., and G. S. Payne, A theoretical study of the ice accretion process, *Q. J. R. Meteorol. Soc.*, *93*, 195–213, 1967.

Macklin, W. C., and G. S. Payne, Some aspects of the accretion process, *Q. J. R. Meteorol. Soc.*, *94*, 167–175, 1968.

Macklin, W. C., and G. S. Payne, The spreading of accreted droplets, *Q. J. R. Meteorol. Soc.*, *95*, 724–730, 1969.

Mitchell, D. L., and D. Lamb, Influence of riming on the chemical composition of snow in winter orographic storms, *J. Geophys. Res.*, *94*(D12), 14,831–14,840, 1989.

Myerson, A. S., and D. J. Kirwan, Impurity trapping during dendritic crystal growth, 1, Computer simulation, *Ind. Eng. Chem. Fundam.*, *16*(4), 414–420, 1977.

Pfann, W. G., *Zone Melting*, 310 pp., John Wiley, New York, 1966.

Pruppacher, H. R., and J. D. Klett, *Microphysics of Clouds and Precipitation*, 954 pp., Kluwer Acad., Norwell, Mass., 1997.

Sato, K., T. Daimon, N. Takenaka, H. Bandow, and Y. Maeda, Decrease of solute in the aqueous solution in the freezing process, in *Proceedings from the NIPR Symposium on Polar Meteorology and Glaciology*, vol. 10, pp. 138–148, Natl. Inst. of Polar Res., Tokyo, 1996.

Schwartz, S. E., Mass-transport considerations pertinent to aqueous phase reactions of gases in liquid-water clouds, in *Chemistry of Multiphase Atmospheric Systems*, edited by W. Jaeschke, pp. 415–471, Springer-Verlag, New York, 1986.

Seinfeld, J. H., and S. N. Pandis, *Atmospheric Chemistry and Physics: From Air Pollution to Climate Change*, 1326 pp., John Wiley, New York, 1998.

Snider, J. R., and J. Huang, Factors influencing the retention of hydrogen peroxide and molecular oxygen in rime ice, *J. Geophys. Res.*, *103*(D1), 1405–1415, 1998.

Snider, J. R., D. C. Montague, and G. Vali, Hydrogen peroxide retention in rime ice, *J. Geophys. Res.*, *97*(D7), 7569–7578, 1992.

Sommerfeld, R. A., C. A. Knight, and S. K. Laird, Diffusion of HNO3 in ice, *Geophys. Res. Lett.*, *25*(6), 935–938, 1998.

Stuart, A. L., Volatile chemical partitioning during hydrometeor freezing and its effects on tropospheric chemical distributions, Ph.D. thesis, Stanford Univ., Stanford, Calif., Aug. 2002.

Tabazadeh, A., and O. B. Toon, The role of ammoniated aerosols in cirrus cloud nucleation, *Geophys. Res. Lett.*, *25*(9), 1379–1382, 1998.

Thibert, E., and F. Dominé, Thermodynamics and kinetics of the solid solution of HNO_3 in ice, *J. Phys. Chem. B*, *102*, 4432–4439, 1998.

Tiller, W. A., and R. F. Sekerka, Redistribution of solute during phase transformations, *J. Appl. Phys.*, *35*(9), 2726–2729, 1964.

Voisin, D., M. Legrand, and N. Chaumerliac, Scavenging of acidic gases (HCOOH, CH3COOH, HNO3, HCl, and SO2) and ammonia in mixed liquid-solid water clouds at the Puy de Dome mountain (France), *J. Geophys. Res.*, *105*(D5), 6817–6835, 2000.

Wang, C., and J. S. Chang, A three-dimensional numerical model of cloud dynamics, microphysics, and chemistry, 3, Redistribution of pollutants, *J. Geophys. Res.*, *98*(D9), 16,787–16,789, 1993.

Wilcox, W. R., Mass transfer in fractional solidification, in *Fractional Solidification*, edited by M. Zief and W. R. Wilcox, pp. 47–112, Marcel Dekker, New York, 1967.

Wolten, G. M., and W. R. Wilcox, Phase diagrams, in *Fractional Solidification*, edited by M. Zief and W. R. Wilcox, pp. 21–46, Marcel Dekker, New York, 1967.

M. Z. Jacobson, Department of Civil and Environmental Engineering, Stanford University, Stanford, CA 94305-4020, USA. (jacobson@stanford.edu)

A. L. Stuart, Center for International Security and Cooperation, Encina Hall E214, Stanford University, Stanford, CA 94305-6165, USA. (astuart@stanford.edu)